27th International Congress
on Sound and Vibration
The annual congress of
the International Institute
of Acoustics and Vibration (IIAV)

11-16 July, 2021

ICSV27

Annual Congress of the International Institute of Acoustics and Vibration (IIAV)

CONTROL OF VIBRATION IN A PLATE USING ACTIVE ACOUSTIC BLACK HOLES

Kristian Hook
ISVR, University of Southampton, Southampton, UK
e-mail: K.Hook@soton.ac.uk
Jordan Cheer
ISVR, University of Southampton, Southampton, UK
email: J.Cheer@soton.ac.uk
Stephen Daley
ISVR, University of Southampton, Southampton, UK
email: S.Daley@soton.ac.uk

Acoustic Black Holes (ABHs) have been shown to provide significant vibration damping in both beams and plates. Although effective, the performance of ABHs has been shown to be limited at lower frequencies, where the local modes of the ABH dominate the structural response. Previously, integrating active control into the taper of an ABH beam termination has been explored and the resulting active ABH (AABH) has been shown to perform very well; namely it has been shown that the reflection coefficient can be controlled almost perfectly over a broad range of frequencies. In this paper, active components have been integrated into ABHs embedded in a plate and a multichannel feedforward control strategy has been presented that can be used to control the global structural response of the plate. It has been shown that active control can be used to address the low frequency performance limit of the embedded AABHs which, combined with the passive damping provided by the ABH effect, demonstrates that AABHs can be used as an effective broadband vibration control solution. It has also been shown that the AABHs provide better coupling with the secondary sources, therefore reducing the energy required to implement active control.

Keywords: Acoustic Black Hole, Feedforward, Active Control, Vibration, Plate

1. Introduction

In structures, acoustic black holes (ABHs) are tapered features that can provide effective damping at frequencies above the first local taper mode. In a plate, ABHs have been realised as both surface-attached vibration dampers [1, 2, 3] and embedded damping features [4, 5, 6, 7, 8, 9, 10, 11, 12]. This paper will focus on the embedded features, for which an example is shown in Figure 1. This ABH has been defined using the height profile

$$h(r) = \varepsilon \left(1 - \frac{r}{r_{abh}}\right)^{\mu} + h_{min}, \tag{1}$$

where $\varepsilon = h_{plate} - h_{min}$ is a scaling factor, $h_{min} = h_{plate} - h_0$ is the minimum thickness of the ABH, r_{abh} is the radius of the ABH and μ is the power law used to define the taper gradient.

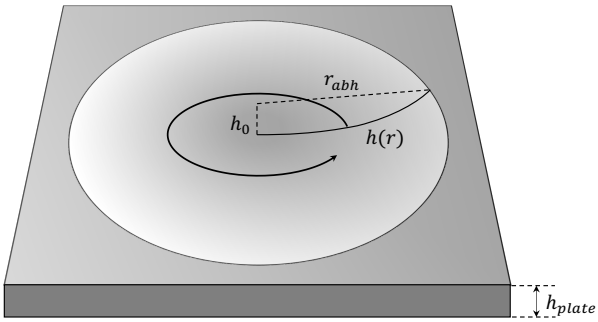

Figure 1: A diagram showing how an ABH is embedded into a plate.

The low frequency performance of a plate with embedded ABHs has been shown to be characterised by the local ABH modes [9, 13] which, when excited, produce narrow bands of absorption in the structural response. At frequencies below the first local ABH mode, the structural response is similar to a constant thickness plate. The frequency of the first local ABH mode has, therefore, been referred to as the cut-on frequency of an ABH and can be estimated as the frequency at which the flexural wavelength becomes comparable to the length of the ABH taper [14, 15]. As frequency increases, the modal density and overlap increases [13, 16], which improves the broadband absorption of the ABH. Although the cut-on frequency of an ABH could be reduced by increasing the size of the ABH, this is not always practical due to constraints on the size and weight of the host structure.

An active solution to this problem has been presented for an active ABH (AABH) beam termination in [17], where it has been shown that a feedforward wave-based control strategy can be applied to control the reflection coefficient of the AABH. For a plate with embedded ABHs, the reflection coefficient with respect to structural waves is less obviously defined and, therefore, previous research on ABHs embedded in plates has focused on different structural metrics, such as surface mobility [1, 9] and mean-squared acceleration/velocity [5, 6, 18].

This paper presents an investigation into the performance benefits of embedding AABHs into a plate. The experimental setup is presented in Section 2 and a multichannel feedforward control strategy, which can be used to control the vibration of the plate, is presented in Section 3. This control strategy has been implemented offline and the results are presented in Section 4. Finally, the conclusions of this work are presented in Section 5.

2. Experimental Setup

A diagram of the experimental setup used to investigate the performance of a plate with five embedded AABHs is shown in Figure 2 and photos of the setup are shown in Figure 3. In addition, the dimensions of the setup and some information about the damping material and piezoelectric patches is shown in Table 1. The aluminium plate has been bolted onto the top surface of a perspex box using a metal edge clamp, which reduces the effective surface area of the plate to 412 mm by 312 mm. The shaker has been connected to the underside of the plate using a stinger and the accelerometers have been attached to the top surface of the plate in a grid with a separation of 6 cm. The layout of these ABHs has been based on the layout of control actuators presented in [19], where it is shown that this arrangement of actuators can be used to effectively control the low order modes of a plate with similar dimensions. In addition, this layout of ABHs is similar to a segment of the 13 ABH plate used in [11], which was shown to perform similarly to a plate with a more dense layout of ABHs. Each of the ABH indentations has

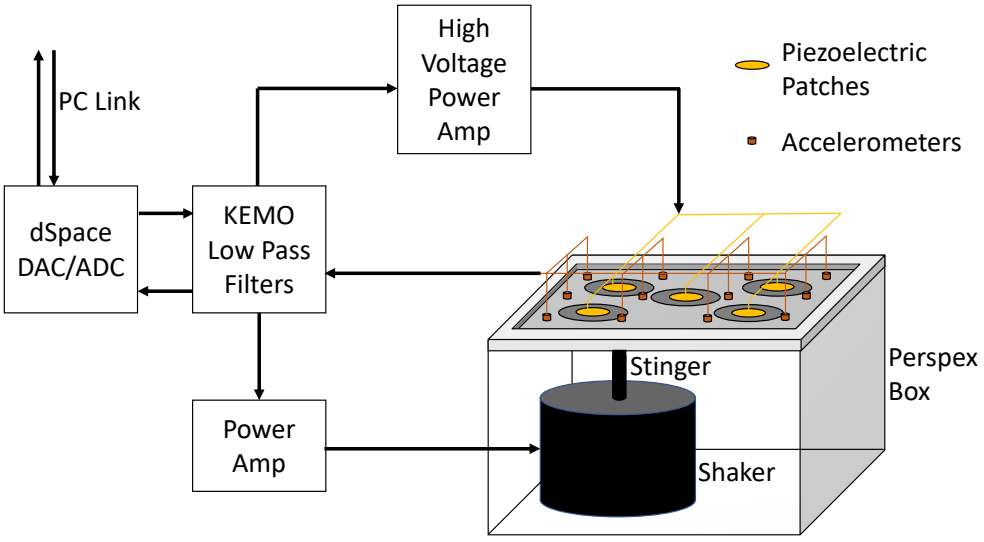

Figure 2: The plate mounted on a perspex box that can be driven by both the shaker and each of the piezoelectric patches attached to the ABHs. A high voltage amplifier is required to drive the piezoelectric patches and low pass filters have been used for signal anti-aliasing and reconstruction.

been defined by revolving the 2D taper described in Equation 1 about the tip and removes approximately 68 g of aluminium from the plate, resulting in a total of 340 g removed from the plate.

For each the ABHs, Henley's yellow compound [20] has been applied to the tapered surface (covering the indentations shown in Figure 3(b)) and piezoelectric patches [21] have been attached to the flat side, co-located with the centre of the ABH (see Figure 3(a)), to reduce pre-stress. The central location also gives better coupling between the piezoelectric patch and the plate due to the thin region of the ABH. The piezo patches have been custom made by PI ceramic, but share the same operating characteristics and thickness as the P-876.A12 patch shown in [21] and have a cut-on frequency of 250 Hz. As discussed in Section 1, the cut-on frequency of an ABH can be estimated as the frequency at which the structural wavelength becomes comparable to the size of the ABH [9, 15, 14], which in this case can be calculated as approximately 1.4 kHz.

Two sampling frequencies have been used. The first, 22 kHz, has been used to measure the broad-

Table 1: Information about the plates and treatments used in the experimental setup.

Variable	**Value**
Plate length	475 mm (412 mm with clamp)
Plate width	375 mm (312 mm with clamp)
Plate height	6 mm
ABH radius	50 mm
ABH minimum height	0.5 mm
ABH power law	3
Henley's damping mass per ABH	17 g
Piezoelectric patch mass	2 g (4 g including resting wire mass)
Piezoelectric patch radius	25 mm
Piezoelectric patch height	0.5 mm

band response of the plate and the second, 4 kHz, has been used to implement the feedforward control strategy that will be described in Section 3. The low-pass anti-aliasing filters have been set with a cut-off frequency of 10 kHz, which is lower than the Nyquist sampling limit imposed by the sensor separation. Using each respective sampling frequency, the shaker and each piezoelectric patch have been driven with white noise and the frequency responses measured at each accelerometer have been calculated using the H1 estimator. To provide contextualisation for the results, another experimental setup has been implemented using a constant thickness plate with the same amount and distribution of damping material and the same active components. The feedforward active control strategy described in Section 3 has also been implemented using the constant thickness active plate and the results for both plates are presented in Section 4.

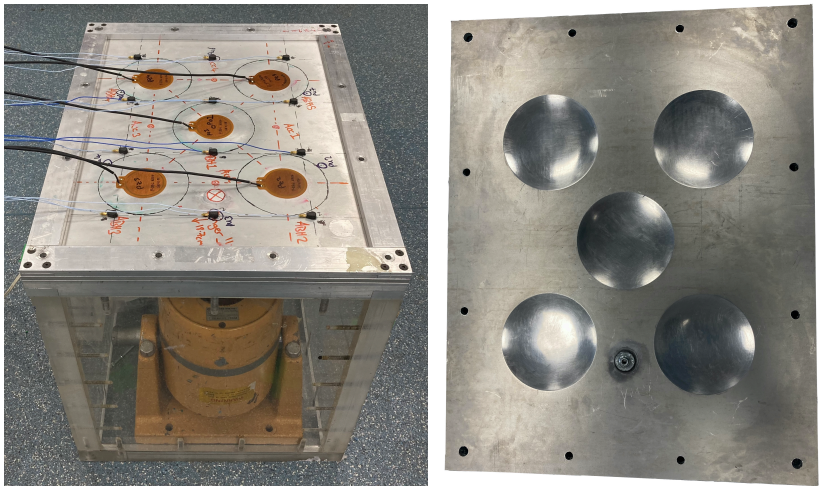

(a) Piezo and accelerometer locations (b) Undamped ABHs

Figure 3: The experimental setup used to measure the structural responses of the plate with embedded ABHs and the constant thickness plate.

3. Controller formulation

A block diagram of the feedforward control system used in this study is shown in Figure 4. The reference signal, x is taken from the signal that is used to drive the shaker and thus a perfect reference signal is assumed in this case. The reference signal is filtered by $\widehat{\boldsymbol{G}}$, which is the matrix of estimated plant responses between the voltage inputs to the piezoelectric patches and the output signals from the accelerometers. The filtered reference signals and the error signals from the accelerometers are then used to update the controller, $\boldsymbol{W}$. The reference signal is filtered by the controller to generate the vector of control signals, $\boldsymbol{u}$, which are used to drive the piezoelectric patches to minimise the primary disturbance. In order to assess the optimum performance of this feedforward control strategy, the optimum matrix of controller coefficients can be calculated offline by following the derivation shown in Section 5.2.1 of [22]. This derivation gives the optimum set of control filter coefficients that can be used to minimise the sum of the squared error signals as

$$\boldsymbol{w}_{\text{opt}} = -\left\{\mathrm{E}\left[\boldsymbol{R}^{\mathrm{T}}(n)\boldsymbol{R}(n)\right] + \beta\mathbf{I}\right\}^{-1}\left[\boldsymbol{R}^{\mathrm{T}}(n)\boldsymbol{d}(n)\right], \tag{2}$$

where E is the expectation operator, $\boldsymbol{R}$ is the matrix of filtered reference signals, $\boldsymbol{d}$ is the vector of disturbance signals, $\mathbf{I}$ is the identity matrix and β is a positive control effort coefficient-weighting parameter,

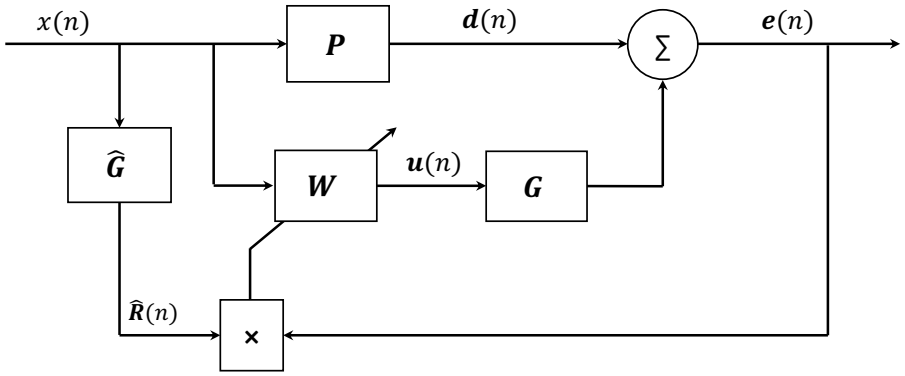

Figure 4: A block diagram showing the feedforward control system that has been used to control the structural vibration of the plate with AABHs.

which has a number of practical benefits [22] and has been included here to enable a constraint to be imposed on the peak-to-peak amplitude of the control signals.

4. Control Performance

The control strategy described in Section 3 has been implemented offline between 400 Hz and 2 kHz to determine the performance of each of the plates under ideal conditions. This frequency range has been chosen because it captures the resonances that fall above the cut-on frequency of the piezoelectric patches, but below the frequency at which the passive damping begins to becomes effective. The plant responses were modelled using 128 FIR filter coefficients and the control filter was set to contain 32 FIR filter coefficients. These values have been chosen because increasing the number of coefficients in either filter gave negligible increase in the plant model accuracy or broadband average attenuation. Each plate has been driven with a white noise disturbance signal between 0 Hz and 10 kHz. The results are presented in terms of the structural response of each plate without damping, with damping and with damping and active control. In addition, the control effort required for each plate is presented over the frequency range that active control has been implemented.

Table 2: The mean broadband structural response of each plate for each of the different control configurations.

Plate type	**Undamped without control**	**Damped without control**	**Damped with control**
ABHs	27 dB	24 dB	22 dB
Constant thickness	28 dB	26 dB	25 dB

From the results presented in Figure 5, it can be seen that without damping both plates exhibit a similar structural response, which is reflected by the similar undamped mean broadband level presented in Table 2. When the passive damping material and piezoelectric patches are added to the plate with embedded AABHs, it can be seen from the results in Figure 5(a) that the AABHs begin to provide passive damping above approximately 1.4 kHz, which was previously identified as the cut-on frequency of these ABHs. Above 2 kHz, it can be seen that there is considerable damping of the plate. From Table 2, it can be seen that this passive damping equates to a 3 dB reduction in the mean broadband structural response. In

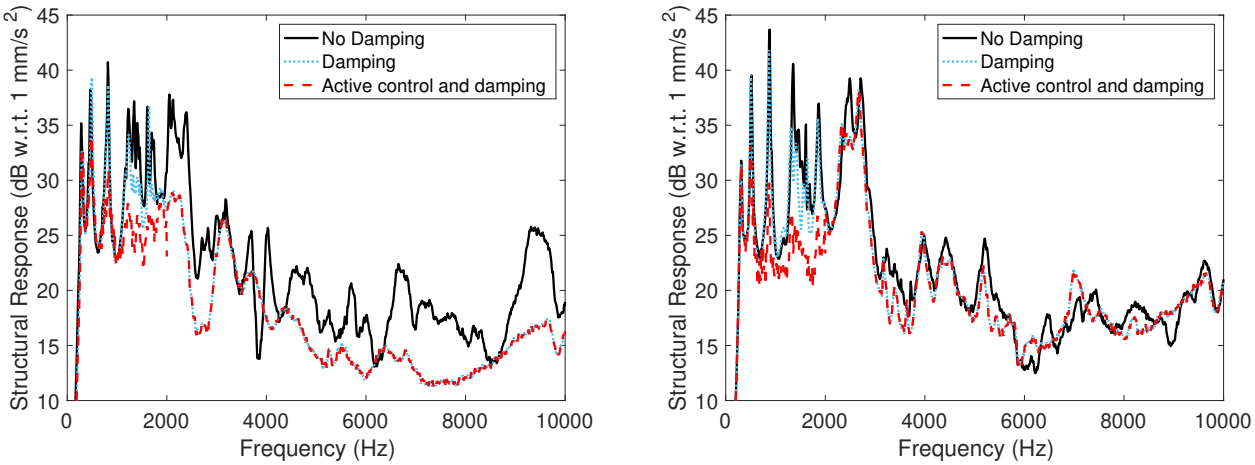

(a) Plate with embedded AABHs

(b) Constant thickness plate

Figure 5: The global structural response of each plate with respect to 1 mm/s^2 when no damping is used, when damping is used and when damping and active control are used.

contrast, from the results presented in Figure 5(b), it can be seen that the addition of damping material and piezoelectric patches slightly dampens the structural response of the constant thickness plate, for example at 1.35 kHz or 2.5 kHz, but the level of damping is less than that of the plate with embedded AABHs. This is reflected in the mean broadband structural response, which is still 2 dB higher than the plate with embedded AABHs. When active control is performed on each of the plates, it can be seen that there is a significant reduction in the structural response below 2 kHz for both plates. Specifically, the resonances of each plate are reduced by up to approximately 12 dB. The combination of both active control and damping can be seen to reduce the mean broadband structural response to 25 dB for the constant thickness active plate and 22 dB for the plate with embedded AABHs. The plate with embedded AABHs therefore offers a 3 dB performance advantage over the constant thickness active plate and a 6 dB performance advantage over an untreated constant thickness plate.

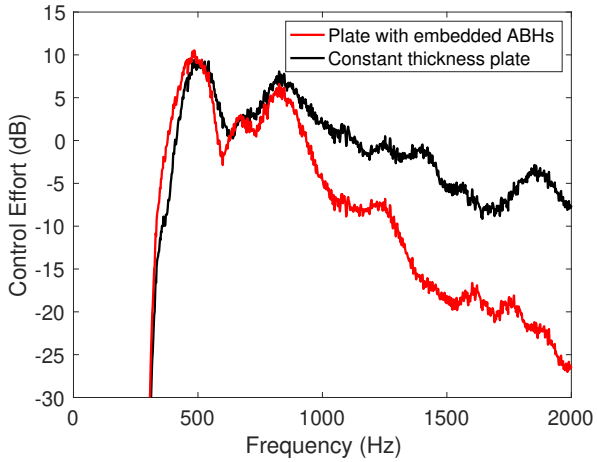

Figure 6: The control effort required for each control case.

In addition to providing more attenuation, the plate with embedded AABHs also requires less energy to implement the active control. This can be seen from the results presented in Figure 6, which show that as frequency increases, the control effort required by the plate with embedded AABHs decreases more than the control effort required by the constant thickness active plate. Over the frequency range presented, the mean control effort is 9 dB lower for the plate with embedded AABHs. The reduced control effort of the AABHs can be attributed to the better coupling between the piezoelectric patches and the thin region of the ABHs. Overall, the results presented in this section have shown that embedding AABHs into a plate provides superior performance compared to a more conventional active treatment and requires a lower control effort.

5. Conclusions

This paper has presented an investigation into the performance of a plate with embedded AABHs and compared it to the performance of a constant thickness active plate. Before control, it has been shown that embedding ABHs into a plate reduces the mass of the plate. In addition, when damping material and piezoelectric patches are attached to the embedded ABHs, they provide significant vibration attenuation above the cut-on frequency of the ABHs. The passive performance has been shown to be superior to a constant thickness plate with the same distribution of damping material and piezoelectric patches.

A global multichannel feedforward control strategy that minimises the sum of the squared error signals has then been implemented using each plate configuration and it has been shown that when active control is performed, the vibration of each plate could be successfully controlled over the active bandwidth. This suitably addresses the low frequency performance limit of the passive ABHs and over the full bandwidth investigated, taking into consideration both the active and passive performance of the plates, it has been shown that the plate with embedded AABHs provides more control. In addition, it has been shown that the thin region of the taper gives better coupling between the piezoelectric patch and the ABH, which reduces the energy required to drive the AABHs. This has practical benefits as cheaper and less powerful active components could be used in practice. In summary, embedding AABHs into a plate offers not only performance advantages in terms of weight and vibration control, but also in terms of energy cost.

Acknowledgements

This work was supported by an EPSRC iCASE studentship (Voucher number 16000058) and an EPSRC Prosperity Partnership (EP/S03661X/1).

REFERENCES

1. S. Park, J.Y. Lee and W. Jeon, "Vibration damping of thin structures using surface-attached spiral acoustic black holes," *Proceedings of Inter-Noise 2020*, Seoul, Korea, 2020, pp. 1–4.

2. T. Zhou and L. Cheng, "A resonant beam damper tailored with Acoustic Black Hole features for broadband vibration reduction," *Journal of Sound and Vibration*, vol. 430, pp. 174–184, 2018.

3. N. Wang, H. Ji, C. Zhang, Y. Lu, J. Qiu and L. Cheng, "A new type of two-dimensional acoustic black hole-based vibration absorber," *Proceedings of Inter-Noise 2020*, Seoul, Korea, 2020, pp. 1–11.

4. O. Unruh, C. Blech and H.P. Monner, "Numerical and Experimental Study of Sound Power Reduction Performance of Acoustic Black Holes in Rectangular Plates," *SAE International Journal of Passenger Cars-Mechanical Systems*, vol. 8, no. 3, pp. 956–963, 2015.

5. L. Ma and L. Cheng, "Topological optimization of damping layout for minimized sound radiation of an acoustic black hole plate," *Journal of Sound and Vibration*, vol. 458, pp. 349–364, 2019.

6. X. Liu, J. Yuan, H. Liang and Z. Wang, "Study on energy propagation and noise radiation in plates containing the array of acoustic black holes," *Proceedings of Inter-Noise 2020*, Seoul, Korea, 2020, pp. 1–10.

7. H. Ji, X. Wang, J. Qiu, L. Cheng, Y. Wu and C. Zhang, "Noise reduction inside a cavity coupled to a flexible plate with embedded 2-D acoustic black holes," *Journal of Sound and Vibration*, vol. 455, pp. 324–338, 2019.

8. L. Cheng, "Sound radiation and transonic boundaries of a plate with an acoustic black hole," *Journal of the Acoustical Society of America*, vol. 145, no. 1, pp. 164–172, 2019.

9. P.A. Feurtado and S.C. Conlon, "An experimental investigation of acoustic black hole dynamics at low, mid, and high frequencies," *Journal of Vibration and Acoustics*, vol. 138, pp. 1–6, 2016.

10. P.A. Feurtado and S.C. Conlon, "Wavenumber transform analysis for acoustic black hole design," *Journal of the Acoustical Society of America*, vol. 140, no. 1, pp. 718–727, 2016.

11. S.C. Conlon and J.B. Fahnline, "Numerical analysis of the vibroacoustic properties of plates with embedded grids of acoustic black holes," *The Journal of the Acoustical Society of America* vol. 137, no. 1, pp. 447–457, 2015.

12. S.C. Conlon and P.A. Feurtado, "Progressive phase trends in plates with embedded acoustic black holes," *The Journal of the Acoustical Society of America* vol. 143, no. 2, pp. 921–930, 2018.

13. K. Hook, J. Cheer and S. Daley, "A Parametric Study of an Acoustic Black Hole on a Beam," *The Journal of the Acoustical Society of America*, vol. 145, no. 6, pp. 3488–3498, 2019.

14. O. Aklouche, A. Pelat, S. Maugeais and F. Gautier, "Scattering of flexural waves by a pit of quadratic profile inserted in an infinite thin plate," *Journal of Sound and Vibration*, vol. 375, pp. 38–52 2016.

15. A. Pelat, F. Gautier, S.C. Conlon and F. Semperlotti, "The acoustic black hole: A review of theory and applications," *Journal of Sound and Vibration*, vol. 476, pp. 1–24 2020.

16. V. Denis, A. Pelat, F. Gautier and B. Elie, "Modal overlap factor of a beam with an ABH termination," *Journal of Sound and Vibration*, vol. 333, no. 12, pp. 2475–2488, 2014.

17. J. Cheer, K. Hook and S. Daley, "Active feedforward control of flexural waves in an Acoustic Black Hole terminated beam," *Smart Materials and Structures* vol. 30, no. 3, pp. 1–14, 2021.

18. L. Ma, H-W. Dong and L. Cheng, "An alternative and optimized thickness profile of an acoustic black hole plate," *Journal of Sound and Vibration*, vol. 486, pp. 1–17, 2020.

19. J. Rohlfing, P. Gardonio and D.J. Thompson, "Comparison of decentralized velocity feedback control for thin homogeneous and stiff sandwich panels using electrodynamic proof-mass actuators," *Journal of Sound and Vibration*, vol. 330, no. 20 pp. 4661–4675, 2011.

20. W.T. Henley, "Yellow plastic compound," `https://www.wt-henley.com/cable_accessories-green_and_yellow_plastic_compound.html`, 2021 (Last Accessed: 16/03/2021).

21. PI Ceramic, "PI876.A11 piezo patch," `https://static.piceramic.com/fileadmin/user_upload/physik_instrumente/files/datasheets/P-876-Datasheet.pdf`, 2021 (Last Accessed: 16/03/2021).

22. S.J. Elliott, "Signal Processing for Active Control," *Academic Press*, London, 2001.